High-pressure, high-temperature phase diagram of InSe: A comprehensive study of the electronic and structural properties of the monoclinic phase of InSe under high pressure

D. Errandonea,[1,*] D. Martínez-García,[1] A. Segura,[1] A. Chevy,[2] G. Tobias,[3,4] E. Canadell,[3] and P. Ordejon[3]
[1]*Departamento de Física Aplicada-ICMUV, Universitat de València, Edificio de Investigación, c/Dr. Moliner 50, 46100 Burjassot (Valencia), Spain*
[2]*Physique des Milieux Condenses, Universite P. et M. Curie, 75252 Paris, Cedex 05, France*
[3]*Institut de Ciència dels Materials de Barcelona, CSIC, Campus de la UAB, 08193 Bellaterra (Barcelona), Spain*
[4]*Inorganic Chemistry Laboratory, University of Oxford, South Parks Road, OX1 3QR Oxford, United Kingdom*
(Received 9 January 2006; revised manuscript received 2 May 2006; published 6 June 2006)

We report on an investigation of the high-pressure, high-temperature phase diagram of InSe. We optically observed the phase transition from the rhombohedral polytype (InSe-I) to the monoclinic phase (InSe-II) and determined the phase boundary up to 10 GPa. High-pressure resistivity measurements were performed to complement the optical measurements. Monoclinic and cubic InSe (InSe-III) were observed to be metastable around 14.5 GPa and 420 K, and evidence suggesting the existence of an as yet unidentified new high-pressure and high-temperature phase was found. By means of optical absorption measurements on InSe-II samples, we observed that InSe-II is a semiconducting phase. It has an absorption coefficient about ten times larger than InSe-I at the absorption edge, which shifts upon compression to low energies. These results were analyzed under the light of first-principles band-structure calculations. We also determined the refractive index of InSe-II and its pressure evolution. Finally, Raman and x-ray diffraction measurements were performed in recovered InSe-II samples, being its crystalline structure refined and its phonon modes determined.

DOI: 10.1103/PhysRevB.73.235202 PACS number(s): 71.20.Nr, 78.40.Fy, 62.50.+p, 78.20.Bh

I. INTRODUCTION

The III-VI semiconductor compounds—InSe, GaSe, GaS, and GaTe—have gained attention in recent years because of their interesting optical properties[1–4] and the possibility of preparing high-quality thin films opened by the so-called van der Waals epitaxy.[5–7] These compounds present an anisotropic crystalline structure with layers formed by two deformed sublayers of hexagonal symmetry held together by strong covalent bonds perpendicular to the layers [see Fig. 1(a)]. The weaker bonding between the layers is of the van der Waals type and leads to the existence of different polytypes. In particular, the semiconductor indium selenide (InSe) crystallizes at ambient conditions in a layered phase, γ-polytype (InSe-I), which belongs to the space group C_{3v}^5 (R3m).[8] The optical properties,[9–15] lattice dynamics,[16,17] and transport properties[18–23] of InSe under compression have been widely investigated. Regarding the structural behavior, it is known that at high-pressure and room-temperature (RT) InSe undergoes a transition toward a NaCl-like cubic phase (InSe-III) and becomes metallic at approximately 10 GPa.[24,25] In addition, at high-pressure and high-temperature the layered γ-polytype of InSe transforms into a monoclinic structure (InSe-II), believed to be nonlayered, being its space group C_{2h}^1 (P2/m) (Ref. 26) [see Fig. 1(b)]. The existence of this phase was first reported by Vezzoli,[27] who obtained the monoclinic phase of InSe by heating for 20 h a crystal of the layered γ-polytype of InSe at 520 K under 4 GPa.[27] Subsequently, Ferlat *et al.*[28] also observed that InSe-I transforms into InSe-II at 620 K and 1 GPa.[28] However, the phase boundary between both phases has not being systematically studied yet. On the other hand, it is known that InSe-II can be quenched to ambient conditions.[26,27] In spite of that, with the exception of a Raman study,[29] very little has been done to know the electronic properties of InSe-II. In particular, the optical absorption and the refractive index of phase II of InSe and their behavior upon compression remains unknown today. The aim of this paper is to study both the high-pressure high-temperature phase diagram of InSe and to determine the electronic properties of InSe-II. After describing the experimental method and the details of the band structure calculations in Sec. II, we will present the experimental results in Sec. III. The electronic structure of InSe-II will be also discussed.

II. EXPERIMENTAL AND THEORETICAL CALCULATION METHODS

A. Experimental procedures

The optical studies were performed in an externally heated membrane diamond-anvil cell (DAC) using thin InSe monocrystals, which were cleaved perpendicular to the [001] direction from an ingot grown by the Bridgman method from a nonstoichiometric $In_{1.05}Se_{0.95}$ melt.[30] Typically, samples of 100×100 μm^2 size and 0.5–3 μm thickness were loaded into a 200 μm diameter hole drilled on a 50 μm thick Inconel gasket and inserted between the 500 μm culet diamond of the DAC. In the reported experiments, silicone oil was used as pressure transmitting medium; the use of a 4:1 methanol–ethanol mixture as a pressure transmitting medium was discarded because we observed that under this medium InSe decomposes at high temperatures. Temperature was increased up to 700 K using an electric heating sleeve, which surrounds the DAC body, and was measured using a K-type thermocouple. The R_1 photoluminescence line of ruby (Ref. 31) and the $^7D_0$-$^5F_0$ fluorescence of $SrB_4O_7:Sm^{2+}$ (Ref. 32) were used to determine the pressure.

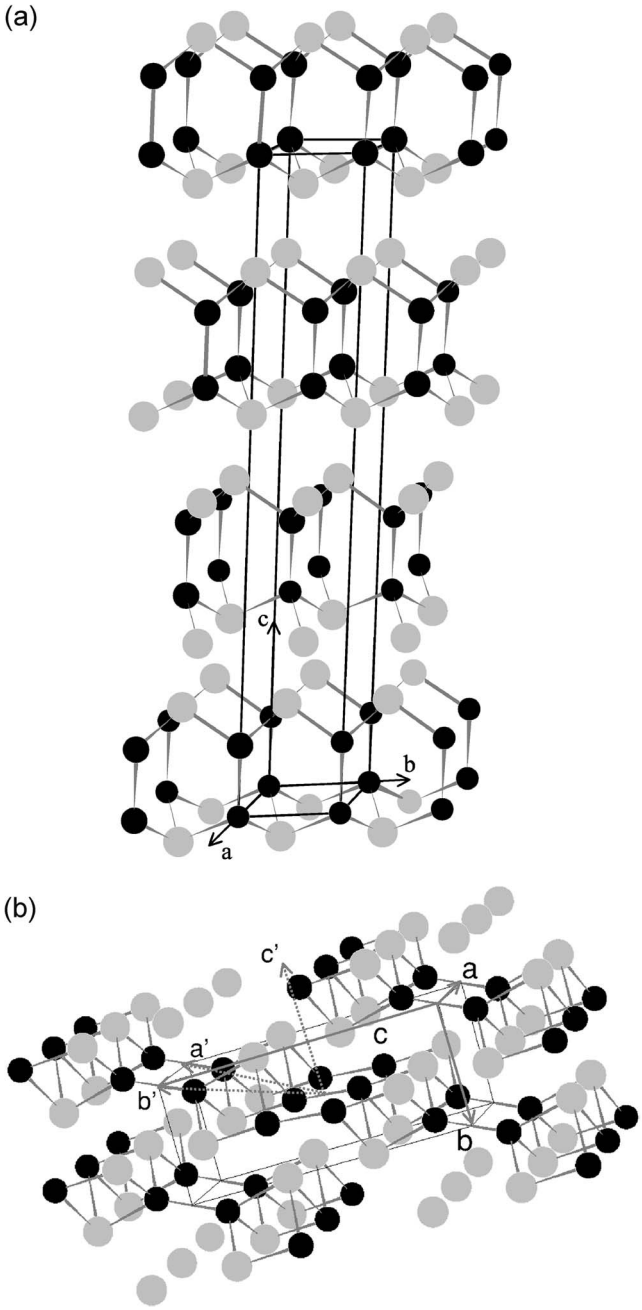

FIG. 1. Schematic view of the crystalline structure of (a) the γ-polytype (InSe-I) and (b) the monoclinic phase of InSe (InSe-II). Black circles represent the In atoms and gray circles the Se atoms. The atomic bonds inside the layers are shown as gray solid lines. The structure of InSe-II is shown in a different perspective to better illustrate the laminar characteristic of this phase. The unit cells are shown with their vector bases $(\vec{a},\vec{b},\vec{c})$ and the primitive unit cell of InSe-II is also shown with its vector bases $(\vec{a}',\vec{b}',\vec{c}')$.

The InSe-I to InSe-II phase boundary was determined by means of optical observation. At the transition, the samples of InSe become darker because their absorption increases by nearly one order of magnitude. InSe-II can be also easily differentiated from InSe-III since [in spite of the large absorption coefficient (α) of InSe-II] light is transmitted through the very thin samples used to conduct our experiments, whereas InSe-III becomes completely opaque because of its metallic character.[24,25] On the other hand, we took advantange of the fact that the InSe-I to InSe-II phase transition is nonreversible and recovered several InSe-II samples in order to study the optical properties of this phase. The transmittance spectra of these samples were measured in the DAC using the sample-in sample-out method in the pressure range up to 15 GPa and from 300 to 700 K. The absorption coefficient was obtained from the transmittance, the sample thickness, and the sample reflectivity calculated from the refractive index (see Ref. 13 for details). The sample thickness was measured from the interference fringe pattern of the ambient-pressure phase and considered not to change after the InSe-I to InSe-II transition. To better determine the band gap of InSe-II, we also performed transmittance measurements at low temperature down to 25 K in a helium closed-cycle cryogenic system.

The recovered InSe-II samples were also used to determine the refractive index of this phase and its pressure dependence. The refractive index was measured by analyzing the interference fringes of the transmittance spectrum using the interference condition $2n(\lambda)d=k\lambda_k$, where $n(\lambda)$ is the refractive index, d is the sample thickness, $k=1,2,3,\ldots$ is the interference order, and λ_k is the wavelength at the maximum corresponding to that order. At ambient conditions, the refractive index was obtained from midinfrared transmittance measurements carried out with a Perkin-Elmer 1600 Fourier transform (FT) infrared microscope. The pressure evolution of the refractive index was determined from transmittance measurements performed in the 800–1300 nm wavelength range. The effects of sample tilting and the variation of sample thickness with pressure were neglected.

With the aim of verifying that the high-pressure and high-temperature phase we observed in the optical measurements was indeed InSe-II, we also synthesized a large InSe-II sample using a Bridgman cell. This sample was obtained at conditions similar to those of the InSe-II samples recovered from the DAC experiments. The Bridgman cell employed for this experiment has been described in detail in Ref. 22. In the present case, the system was improved by using internal graphite disks as heating elements and molybdenum foils, with very high melting temperatures,[33] to apply the current to the heaters. Therefore, by applying a 60 A current, we were able to obtain temperatures higher than 840 K. The temperature was measured using a K-type thermocouple and the pressure was determined by the calibration of the applied load.[34,35] Pressure effects on the thermocouple electromotive force were neglected.[36] The conditions of this experiment were 1 GPa and 700 K, which were held for 1 h. The recovered sample was analyzed by Raman spectroscopy and x-ray powder diffraction to unequivocally establish that the recovered samples correspond to the InSe-II phase. Raman measurements were performed in the backscattering geometry by means of a Bruker RFS 100/S FT-Raman spectrometer. Radiation of 946 nm from a Nd:YAG laser was used for excitation. X-ray diffraction (XRD) experiments were carried out with a Seifert XRD 3003 TT diffractometer using Cu $K\alpha$ monochromatic radiation ($\lambda=1.54$ Å).

Finally, resistivity and Hall effect measurements were also performed in the Bridgman cell in order to determine

the Phase I to Phase II phase boundary up to 1 GPa and 850 K. The tin-doped InSe samples employed for these measurements were typically 150 μm in thickness and 4 $\times 4$ mm^2 in size. Indium or silver (Ag) contacts were vacuum evaporated on the corners of the samples in the van der Pauw configuration [37] Silver wires of 200 μm in diameter were used as electrical leads, being soldered with high-purity indium to the evaporated indium (or silver) electrodes.

B. Band structure calculations

The calculations were carried out using a numerical atomic orbitals (NAO) density-funtional theory (DFT) approach.[38] This method is designed for efficient calculations in large systems and implemented in the SIESTA code.[39] We have used the local density approximation to DFT and, in particular, the functional of Perdew and Zunger.[40] Only the valence electrons are considered in the calculation, with the core being replaced by norm-conserving scalar relativistic pseudopotentials[41] factorized in the Kleinman-Bylander form.[42] Nonlinear partial-core corrections were used to describe the exchange and correlation in the core region.[43] We have used a split-valence double-ζ basis set including polarization orbitals for all atoms as obtained with an energy shift of 250 meV.[44] The energy cutoff of the real space integration mesh was 300 Ry. The Brillouin zone was sampled using a grid of $(6\times6\times6)$ k points.[45] We checked that the results were well converged with respect to the real space grid, the Brillouin zone (BZ) sampling, and the range of the numerical atomic orbitals.

III. RESULTS AND DISCUSSION

A. P-T phase diagram of InSe

From optical measurements at different pressures and temperatures, we have determined the InSe-I to InSe-II phase boundary in the pressure range from 1 to 10 GPa. In our optical measurements, the nonreversible Phase I to Phase II transition was easily identified above 1 GPa as a clear change in the shape and intensity of the absorption edge. The absorption edge changes its shape and slightly shifts in energy and the absorption coefficient increases by approximately a factor 10 when passing from InSe-I to InSe-II. Figure 2 shows several pictures taken at different P-T conditions in a 1 μm thick InSe sample. There, the changes on the sample when going through the transition can be easily identified [see Figs 2(b) and 2(c)] and it can be also observed that changes on the sample are not reversible [see Fig. 2(d)]. In Fig. 2, the appearance of linear defects (darkest lines) reported in Ref. 25 can be also observed. It is known that the presence of this kind of defect allows the match between different structural phases in a crystal under compression,[46–48] and consequently they may play a precursor role in the InSe-I to InSe-II transition. It is important to note here that individual domains of the InSe-I sample separated from other domains by linear defects would become different crystallites after the InSe-I to InSe-II transition. Therefore, the obtained InSe-II sample had a polycrystalline character in spite of the monocrystalline character of the original InSe-I sample. Figure 3 shows several absorption spectra of InSe collected at conditions similar to the images shown in Fig. 2. There, the typical features of the absorption spectrum of InSe-I can be seen in the spectrum measured at 5.8 GPa and 380 K. In contrast, the spectrum measured at 6.4 GPa and 460 K shows a quite large increase of the absorption of the sample and a shift of the absorption edge toward lower energies. These changes correspond to the changes observed between Figs. 2(b) and 2(c) and indicate the occurrence of the transition from InSe-I to InSe-II. On the other hand, the absorption spectrum measured at 6.4 GPa when decreasing the temperature to 300 K is very similar to that measured at 6.4 GPa and 460 K, confirming the nonreversibility of the phase transition.

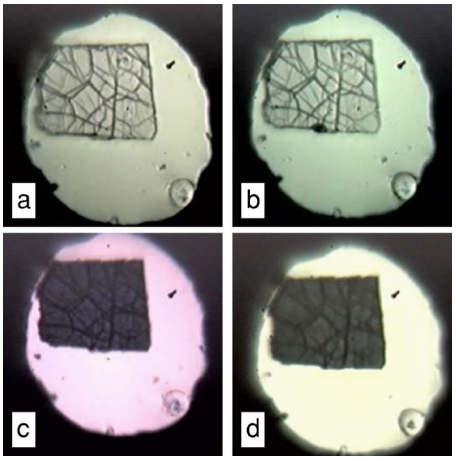

FIG. 2. (Color online) Optical observation of the InSe-I to InSe-II phase transition in a 1 μm thick sample. At the transition, the sample (30×30 μm^2 in size) becomes opaque: (a) InSe-I at 5.7 GPa and 300 K, (b) InSe-I at 6 GPa and 415 K, (c) InSe-II at 6.4 GPa and 460 K, and (d) InSe-II at 6.4 GPa and 300 K [recovered from (c)].

Figure 4 shows the P-T phase diagram we constructed for InSe based upon our own research and previous studies.[24,27–29] Our results are compatible with previous

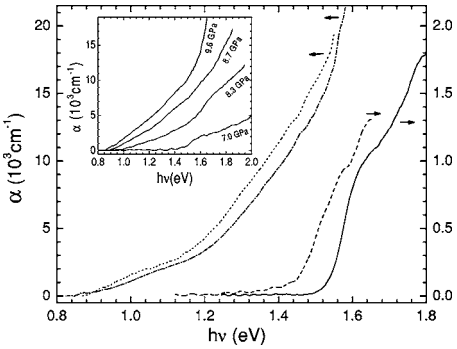

FIG. 3. Comparison of the absorption coefficients of Phases I and II. Solid line: 5.7 GPa and 300 K (InSe-I), dashed line: 5.8 GPa and 380 K (InSe-I), dotted line: 6.4 GPa and 460 K (InSe-II), and dotted-dashed line: 6.4 GPa and 300 K (InSe-II). The inset shows the absorption coefficient (measured in a 2.7 μm thick sample) as a function of pressure at RT illustrating the InSe-I to InSe-II transition.

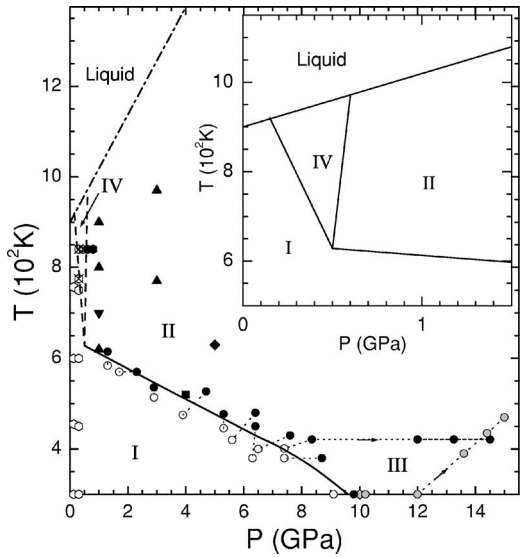

FIG. 4. *P-T* phase diagram of InSe. Circles represent the present optical observations. Solid (empty) circles indicate the stability of InSe-II (InSe-I), and gray circles the stability of InSe-III. The solid line indicates the Phase I—Phase II transition line. The dashed lines are postulated phase boundaries. The dashed-dotted line is the melting curve of InSe (Ref. 28). The dotted lines connect data points measured in the same sample. Black diamond: InSe-II from Iwasaki *et al.* (26), square: InSe-II from Vezzoli *et al.* (27), up triangles: InSe-II from Ferlat *et al.* (Ref. 28), down triangle: InSe-II synthesized in the present work using a large volume press, and gray diamond: InSe-III from Schwarz *et al.* (Ref. 24). The hexagons correspond to the results obtained from the resistivity measurements. Empty hexagons: InSe-I, solid hexagons: InSe-II, and crossed hexagons: InSe-IV. The arrows show two runs following different *P-T* paths showing that, depending on the run, InSe-II or InSe-III is metastable at 14.5 GPa and 420 K. The inset shows a scheme of the low-pressure part of the phase diagram.

works[26–28] and extend the InSe-I to InSe-II transition line to higher pressures. It is important to note here that the solid line plotted in Fig. 4 represents the kinetic transition line rather than the thermodynamic phase boundary. However, in view of the relative high temperature of the Phase I-Phase II transition at low pressures and of the fact that we observed the same transtion also at RT near 10 GPa, it is reasonable to assume that the activation barrier is small in this transition. Then, the observed transition points are expected to be close to the equilibrium line. Therefore, along the discussion of the phase diagram of InSe, we will consider the InSe-I to InSe-II transition line as an equilibrium line.

From the results we obtained from 11 different samples at different *P-T* conditions, we found that above 1 GPa the Phase I-Phase II boundary has a negative slope of nearly −30 K/GPa, and that above 7 GPa it bends toward the pressure axis intersecting the RT isotherm at around 9.5 GPa. The inset of Fig. 3 shows the evolution of the absorption spectrum of InSe at RT from 7 GPa to 9.6 GPa, illustrating how it changes from a spectrum characteristic of InSe-I at 7 GPa to one resembling the absorption spectrum of InSe-II at 9.6 GPa. Above this pressure, the sample becomes completely opaque indicating the transition to InSe-III. The above described facts indicate that at RT the structural sequence of InSe under compression probably is $I \rightarrow II \rightarrow III$, instead of $I \rightarrow III$ as believed until now. The range of stability of Phase II at RT is smaller that 1 GPa, which probably preclude the identification of it in previous studies.[24,25] It is important to note here that the appearance of a new Raman peak beyond 7 GPa was observed in previous Raman measurements carried out on InSe-I.[17] This additional peak was observed from 7 GPa to 10 GPa, and was still observable upon pressure release around 143 cm^{-1} at 1 bar. This frequency coincides with the frequency of the most intense mode of InSe-II,[29] which also suggests that the RT structural sequence of InSe might be $I \rightarrow II \rightarrow III$. It is also important to state the fact that $dT/dP < 0$ at the Phase I to Phase II boundary of the P-T phase diagram, which implies, according to the Clausius-Clapeyron equation[49] ($dT/dP = \Delta V/\Delta S$, where ΔV and ΔS are, respectively, the difference in molar volume and entropy of InSe-I and InSe-II), that Phase II is more dense than Phase I.

Regarding the *P-T* phase diagram below 1 GPa, it is well established in the literature that at 1 bar pressure InSe-I remains stable up to melting. We also observed in our resistivity measurements that Phase I remains stable up to 750 K at 0.3 GPa. In particular, we found that at 0.3 GPa the resistivity (ρ) slowly increases with temperature from 0.12 Ω cm at 300 K to 0.38 Ω cm at 750 K in agreement with the results of our previous studies (see Fig. 5).[22] However, when increasing the temperature above 750 K, a faster increase in the resistivity with temperature is observed (e.g., it goes from 0.38 Ω cm at 750 K to 1 Ω cm at 840 K), being this change related to a decrease in the carrier concentration (n) and a slope change in the carrier mobility (μ). Note that below 750 K, the mobility is proportional to $T^{-1.15}$, in agreement with previous measurements performed in InSe-I.[22] A possible reason for the observed changes in μ and n above 750 K will be given later. On the other hand, upon compression at 840 K, we first observed that all the transport parameters remain nearly constant from 0.3 GPa to 0.55 GPa. However, at 0.6 GPa, an abrupt change in the resistivity was observed which is caused by a decrease in both the carrier concentration and mobility (see Fig. 5). We attributed the abrupt changes observed at 0.6 GPa and 840 K to the stabilization of InSe-II. It is important to note here that after these abrupt changes observed at 0.6 GPa, the transport parameters do not change upon further compression at constant temperature up to 0.8 GPa, which is consistent with the fact that, according to previous XRD experiments,[28] InSe-II is expected to be stable around 0.8 GPa and 840 K. On top of that, the abrupt changes observed in ρ, n, and μ at 840 K above 0.55 GPa were not reversible as expected for the transformation of InSe to the monoclinic phase. Then, if we assumed that below 0.5 GPa and above 600 K, a Phase I to Phase II solid-solid transition takes place, dT/dP would became quite large below 0.5 GPa, causing a large change in the slope of the phase-boundary curve somewhere around 0.5 GPa. This fact is in contradiction with the general principles of thermodynamics, which predict that there are no abrupt changes in the phase boundaries of any two-phase transformation. In our particular case, from Fig. 4 and according to the Clausius-Clapeyron equation[49] (which follows

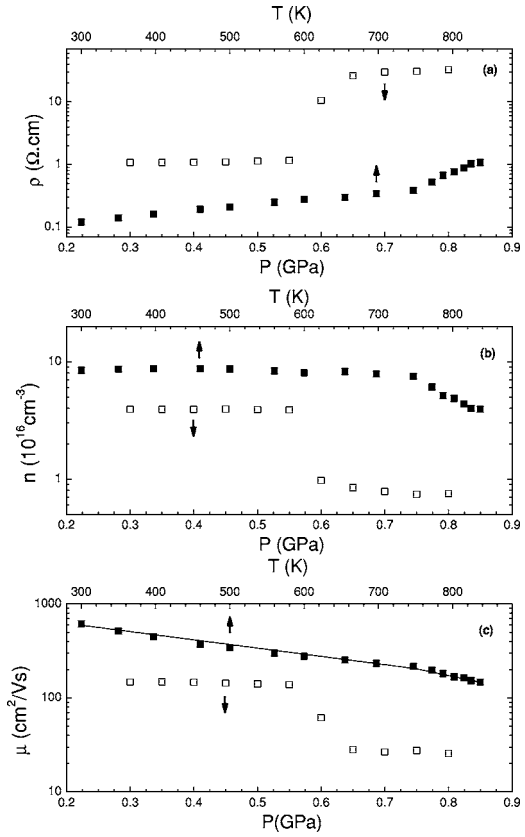

FIG. 5. Resistivity and Hall effect measurements. First, the temperature was increased from 300 K to 840 K at 0.3 GPa, and subsequently the pressure was increased from 0.3 GPa to 0.8 GPa at 840 K. Solid symbols represent the measurements performed at constant load (P=0.3 GPa) at different temperatures. Empty symbols represent the measurements performed at constant temperature (T=840 K) at different pressures.

directly from the Gibbs equality),[50] it is straightforward to conclude that, since usually entropy changes at a solid-solid transition tend to be small, above 0.5 GPa, ΔV is also expected to be small. However, if below 0.5 GPa InSe-I transforms directly to InSe-II, the slope of the phase boundary becomes extremely abrupt, implying a large ΔV, which is quite unrealistic since the volume is an analytical function of P and T and therefore a differential change in P and T cannot produce abrupt changes in ΔV. One possible explanation of the observed stability P-T ranges of InSe-I and InSe-II is the existence of a third phase at play, which we will denote as Phase IV. The existence of this phase between InSe-I and InSe-II below 0.6 GPa and above 650 K would imply that the three phases meet at a triple point near 0.5 GPa and 650 K. The proposed stability range for InSe-IV is shown in Fig. 4. It is important to note here that the rhombohedral γ-phase of InSe (InSe-I) could transform into different hexagonal and rhombohedral layered polytypes under heat treatment at low pressures.[51,52] Therefore, the possible stabilization of any of the other known layered polytypes of InSe is compatible with the three-phase scenario we proposed above. One candidate structure for InSe-IV may be a GaTe-like structure (B2/m).[53] This monoclinic structure is more similar to the rombohedral γ-polytype of InSe (R3m) (Ref. 8) than the monoclinic InSe-II structure (P2/m).[26] Due to the similarities between the B2/m and R3m structures, the GaTe-like structure would suppose a smaller entropy change at the InSe-I to InSe-IV transition than the one at the InSe-I to InSe-II transition. This fact, would explain the large change observed in dP/dT at the I-II-IV triple point. It is important to note here that the changes observed in the transport parameters at 0.3 GPa beyond 750 K take place at P-T conditions similar to those we estimate for the occurrence of the InSe-I to InSe-IV, being that this transition is their possible cause. Validation of the proposed revised phase diagram of InSe can be only obtained by the performance of *in situ* XRD experiments under high-pressure and high-temperature taking advantage of third-generation synchrotron sources.

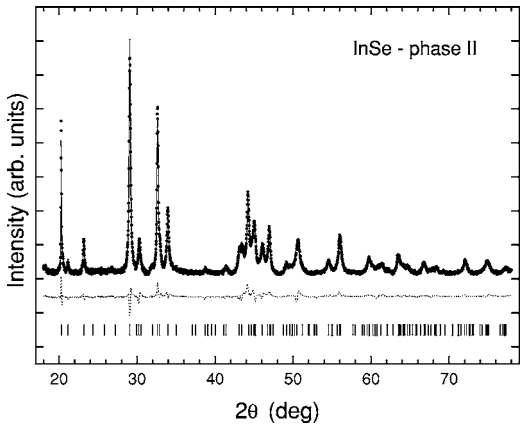

FIG. 6. Powder diffraction patterns of quenched InSe-II at ambient conditions. Black symbols: Observations, solid line: Refined model, and dotted line: Residual. The position of the Bragg reflections is indicated.

Before closing the discussion on the P-T phase diagram of InSe, we would like to mention that when compressing a sample of InSe-II from 8.4 GPa to 14.5 GPa at 420 K we found that it did not transform to InSe-III. On the contrary, when following a different P-T path, starting from InSe-III at 12 GPa and 300 K and going to 14.4 GPa and 430 K, we observed that InSe-III remains stable at the same P-T conditions that we observed InSe-II to be stable by following the 420 K isotherm. Therefore, both phases seems to be metastable at high temperatures at these conditions.

B. X-ray diffraction and Raman measurements

In order to unequivocally conclude that the high P-T phase we observed was the monoclinic phase of InSe, we performed XRD and Raman measurements in a sample of InSe-II quenched in the Bridgman cell from 1 GPa and 700 K. We collected 15 different XRD patterns in the quenched sample covering the 18°–78° 2θ range, and averaged them to perform a Rietveld refinement. Figure 6 shows the averaged XRD pattern. The Rietveld refinement (performed using the POWDERCELL program)[54] of this profile, with the monoclinic P2/m structure reported by Iwasaki *et al.*,[26] is also shown in Fig. 6: R_{WP}=2.26%, R_P=1.72%, $R(F^2)$=2.1% for 128 reflections. For this structure, which has four molecular units contained in the unit cell, we ob-

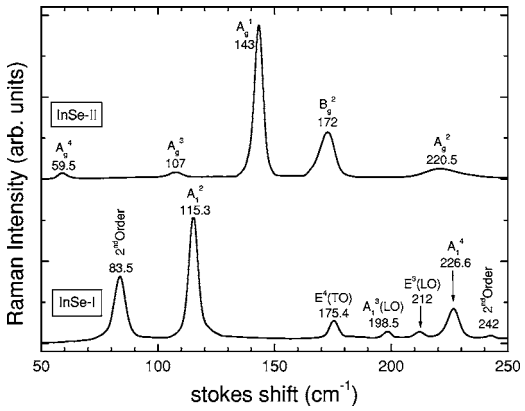

FIG. 7. Raman spectra of InSe-I and InSe-II. The observed zone-center modes are labeled.

tained the following lattice parameters and atomic volume: $a=4.088(4)$ Å, $b=4.655(4)$ Å, $c=10.981(8)$ Å, $\alpha=86.85(3)^\circ$, $V=208{,}5(5)$ Å^3, which differ by less than 1% from those values reported by Iwasaki *et al.*[26] These results unequivocally confirm that the high *P-T* phase we optically observed is the monoclinic phase previously reported in the literature.[26–28] An important fact to note here is that the monoclinic structure of InSe-II, in spite of having been considered until now as a nonlayered structure, is indeed a layered structure as can be seen in Fig. 1(b). This figure shows how the P2/m structure is built up by Se-In-In-Se layers. The main difference between the monoclinic P2/m structure and the rhombohedral γ-polytype is that, in the first one the In-In bonds are parallel to the layers, and in the second one are perpendicular to the layers.

Regarding the Raman measurements, they are also in good agreement with those reported in the literature[29] and confirmed that our samples were transformed to Phase II. Figure 7 shows the Stokes spectra measured for InSe-I and InSe-II. In the spectral range of our measurements, five zone-center phonons of InSe-I can be identified in addition to two overtones. The assignment of these modes is well established in the literature.[55–58] The E^2 mode is not observed because the spectral range of the used spectrometer cannot be extended below 50 cm^{-1}. The energy of the observed Raman peaks is in good agreement with previous results.[17,55–58] The second-order Raman peaks are present in the spectrum because the laser excitation energy is tuned to an optical interband transition. At 1 bar pressure, the 946 nm line of the Nd:YAG laser matches the direct band gap of γ-InSe.[10] InSe-II exhibits a quite different spectrum than that of InSe-I. On it, we can identify another five structures. The measured spectrum is very similar to that reported by Kuroda *et al.*[29] However, in our experiments, we were not able to observe the B_g^1 mode of InSe-II due to the spectral range limitation of our setup. Regarding the mode assignment, we think the assignment of the Raman lines in Ref. 29 is incorrect. Kuroda *et al.*[29] did not seem to realize that the monoclinic unit cell of the InSe-II structure is a nonprimitive unit-cell and therefore they duplicated the number of vibration modes. The primitive unit cell of InSe-II can be constructed by performing the following vector base transformation:

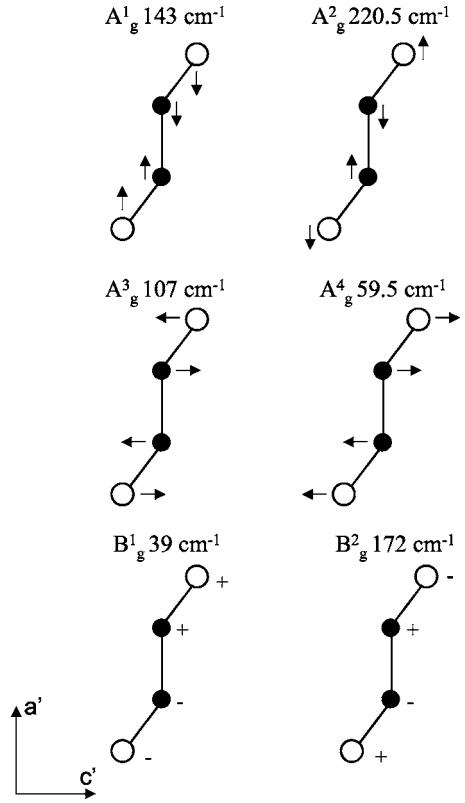

FIG. 8. Schematic representation of the six zone-center Raman active modes. Black circles: In atoms and white circles: Se atoms.

$$\vec{a}' = \frac{\vec{a} - \vec{b} + \vec{c}}{2}, \quad \vec{b}' = \frac{-\vec{a} - \vec{b} + \vec{c}}{2}, \quad \text{and} \quad \vec{c}' = -\vec{b},$$

where $\vec{a}'$, $\vec{b}'$, $\vec{c}'$ is the vector base of the primitive unit cell, and $\vec{a}$, $\vec{b}$, $\vec{c}$ is the vector base of the conventional unit-cell of the P2/m structure; see Fig. 1(b). The primitive cell has two units of InSe instead of four, and therefore InSe-II should have 12 normal modes in contrast to the 24 proposed by Kuroda *et al.*[29] The symmetry of the C^1_{2h} space group leads in InSe-II to six zone-center Raman-active modes following the decomposition:

$$\Gamma = 4A_g + 2B_g.$$

The different vibrations involved in each mode are represented in Fig. 8, together with the present assignment and the measured frequencies. As for the A_g^4 and B_g^1 modes, all Se-In units on each side of the In-In bond vibrate almost rigidly; these modes are expected to have the lowest frequencies. On the other hand, as happens in the γ-polytype of InSe, the vibration perpendicular to the layer involving stretching of the In-In and In-Se bonds is expected to have the highest frequency.

C. Band structure of InSe-II

Figure 9(b) shows the band structure calculated for monoclinic InSe along high symmetry directions of its BZ. A sketch of the monoclinic BZ is shown in Fig. 9(a). In order

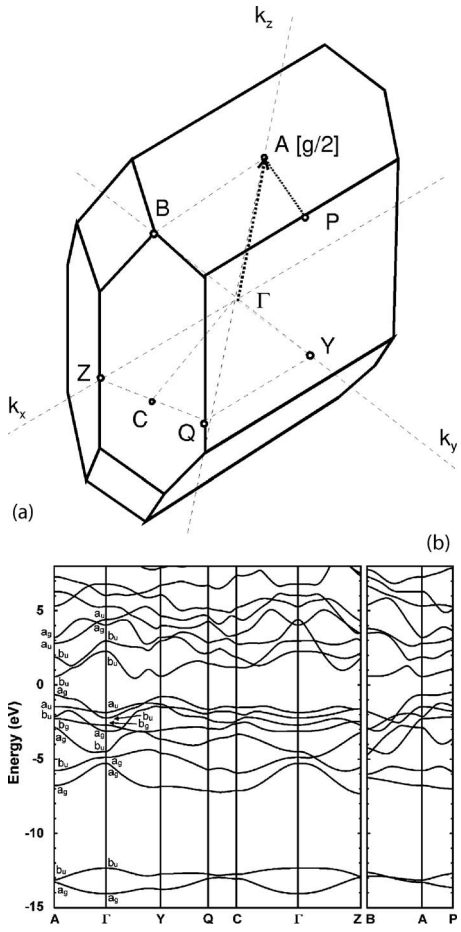

FIG. 9. (a) BZ of InSe-II and (b) band structure of InSe-II at 1 bar as calculated by the NAO-DFT method. $E=0$ corresponds to the Fermi energy level. In (a), g represents the reciprocal vector $\vec{c}'^{*}=2\pi(\vec{a}'\times\vec{b}')/[\vec{a}\cdot(\vec{b}'\times\vec{c}')]$.

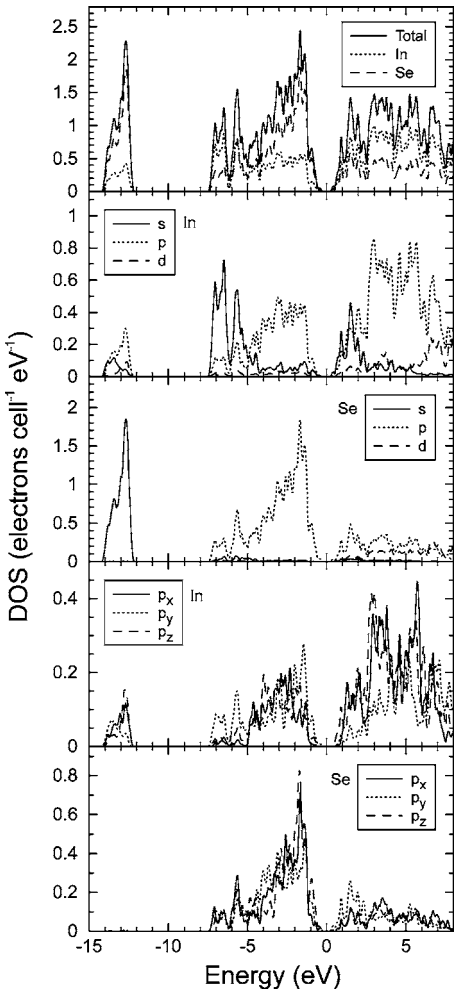

FIG. 10. Total and projected density of states of InSe-II onto the different atomic sites and the different orbital contributions.

to figure out the orientation of the BZ with respect to the crystal structure given in Fig. 1(b), one should consider that the Γ-A direction corresponds to the axis perpendicular to the layer plane (which corresponds to the dotted-line polygon). In that plane, the lines Γ-Z (binary axis) and Γ-Y are perpendicular and parallel to the In-In bonds. Consequently, the mirror plane of the point group corresponds to the k_x-k_y plane. As in γ-InSe, the primitive unit cell of monoclinic InSe contains two InSe units. Then, the lowest lying 9 bands are filled by the 18 valence electrons of the unit cell. Figure 10 shows the density of states and its orbital decomposition, with the previously defined axis orientation.

Even if the lower symmetry of monoclinic InSe leads to much stronger orbital mixing, there are some similarities between the electronic structure of both InSe polymorphs: (i) The two lowest lying bands mainly have Se s character, (ii) the following upper band has predominant In s character and corresponds to the In-In covalent bond (molecular bonding σ orbitals), (iii) the following six bands have predominant Se p character, (iv) the upper valence band has, in most of the BZ, predominant Se p_z character and mainly corresponds to the electron pair responsible for the interlayer interactions, (v) the In character dominates in the lowest conduction band (with a stronger participation of s orbitals), although there is also a very sizeable contribution of the Se p orbitals (i.e., antibonding In-Se σ orbitals) (vi) the lowest direct gap occurs at the intersection with the BZ limit of an axis perpendicular to the layer plane including the Γ point, i.e., the A point in the monoclinic BZ or the Z point in the rhombohedral BZ.[13]

In regard to the differences, the first one concerns the matrix element of the electronic dipole associated with the direct gap. While in monoclinic InSe this transition is dipole allowed by the crystal symmetry (A_g to B_u), in γ-InSe it is allowed only for light polarization parallel to the c axis.[13] On the other side, the strong orbital mixing in monoclinic InSe gives rise to many subsidiary maxima in the valence band and minima in the conduction band, making the semiconductor indirect. In this direction, it is interesting to point out that this effect also occurs in InSe when the interlayer interactions are increased and the nonequivalence of the half-layers becomes larger under pressure. Monoclinic InSe is then an indirect semiconductor in which the valence-band maximum (VBM) occurs near the P point in the P-Y line and the conduction-band minimum occurs in the same line, near to the Y point.

The small thickness of the sample studied here and the strong light scattering preclude any estimation of the indirect gap of monoclinic InSe. Conversely, the previous analysis of the band structure allows for a quite well-founded assignment of the observed direct transition, that would correspond to the direct transition at the A point. It is also interesting to notice that in the *A*-*P* direction there are several conduction bands at low energy running parallel to the upper valence band in that direction. This would give rise to a strong direct allowed transition that could correspond to the relatively low-energy Penn gap (between 3 and 4 eV) necessary to account for the large refractive index.

Concerning the pressure evolution, the large interlayer interaction must result in a stronge sensitivity of the upper valence band to pressure. The VBM would shift up under pressure giving rise to a pressure decrease in both the direct gap and the Penn gap (as actually observed).

D. Optical absorption coefficient as a function of pressure and temperature

The absorption edge exhibits two different regions: A low-energy tail, that turns out to be insensitive to pressure and temperature, and a steep high-energy edge, that changes with pressure and temperature. The low-energy tail does not follow the energy dependence expected for an indirect transition. Therefore, it cannot be assigned to the fundamental (indirect) band gap predicted by our calculations. Since the low-energy tail is pressure and temperature independent, it seems more reasonable to attribute this tail to light scattering due to the polycrystalline character of the InSe-II sample. On the other hand, the high-energy edge can be identified as the lowest-energy direct transition allowed in monoclinic InSe. In Fig. 11(a), we present the evolution of the absorption edge of InSe-II at RT from ambient pressure to 4.2 GPa. In the measured spectrum, we have been able to separate the absorption edge from the light diffusion we observed at low energies. In this way, we deduced the pressure shift of the energy of the absorption edge up to 10 GPa.

The inset of Fig. 11(a) gives the pressure dependence of the absorption edge. As in InSe-I, GaSe, and GaTe, the pressure dependence of the band gap is strongly nonlinear. The direct band gap at ambient conditions is 1.8 eV. At low pressures, the band gap shifts to lower energies with a rate of −60 meV/GPa, a larger absolute value than that of InSe (−17 meV/GPa), but close to that of GaTe (−85 meV/GPa).

In Fig. 11(b), we illustrate the evolution of the absorption edge with temperature from 25 K to 300 K. In the inset, we give the temperature dependence of the band gap, which is linear. The temperature coefficient is $dE_g/dT = -0.45$ meV/K.

E. Refractive index under pressure

In Fig. 12, we have depicted the transmittance measured in the medium infrared for an InSe-II sample quenched in a DAC experiment. The transmittance spectrum shown corresponds to a 1 μm thick sample and has been taken with nonpolarized light. From these measurements, we have estimated the refractive index of InSe-II at ambient conditions to be $n=2.82$ in the medium infrared ($\lambda \geqslant 2500$ nm). This value agrees with the value we obtained from near-infrared measurements at $\lambda \geqslant 1100$ nm. We also performed transmittance measurements in the near-infrared in a DAC at several pressures. From these measurements, following the procedure

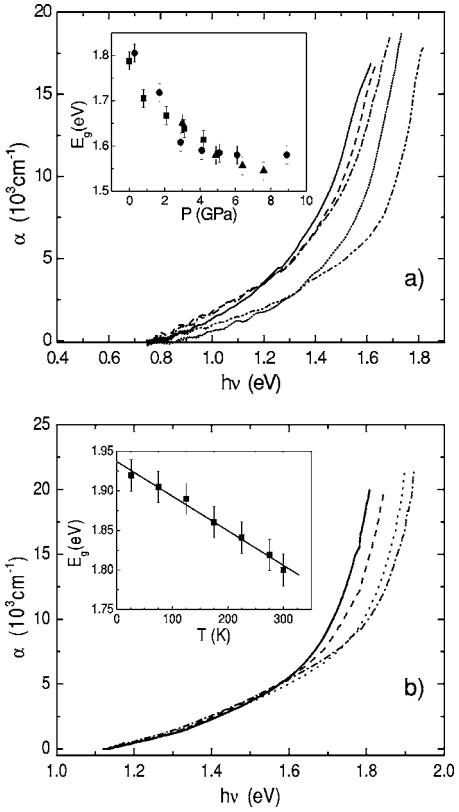

FIG. 11. Pressure (a) and temperature (b) evolution of the experimental absorption coefficient of InSe-II. The insets show the evolution of the band gap with P at 300 K and with T at 1 bar. (a) Solid line: 4.2 GPa, dashed line: 3.1 GPa, dashed-dotted-dashed line: 2.1 GPa, dotted line: 0.8 GPa, and dashed-dotted-dotted-dashed line: 1 bar. (b) Solid line: 300 K, dashed line: 225 K, dotted line: 125 K, and dashed-dotted-dashed: 26 K. Different symbols in the inset of (a) correspond to different samples.

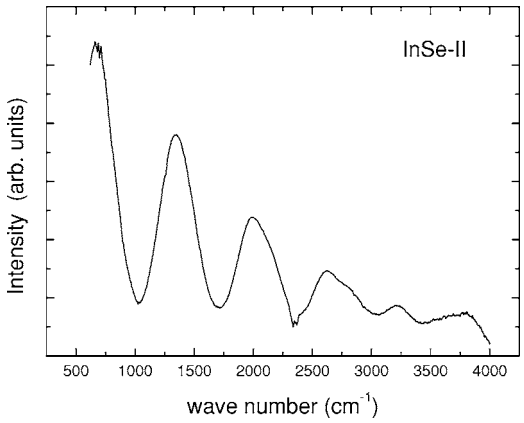

FIG. 12. Medium infrared transmittance of a 1 μm InSe-II sample measured at ambient conditions.

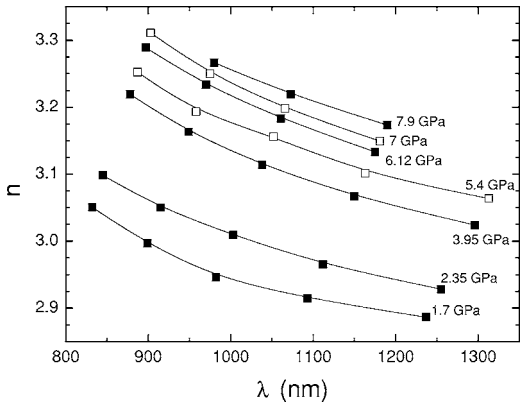

FIG. 13. The refractive index of InSe-II at several pressures as obtained from fringe measurements. Pressures are indicated in the plot. Solid symbols: Up stroke, and empty symbols: Down stroke.

already described in the experimental section, we have been able to obtain the pressure dependence of the refractive index. In Fig. 13, we have represented the refractive index as a function of the wavelength for pressures ranging from 1.7 GPa to 7.9 GPa. At long wavelengths (far away from the electronic transitions determining the refractive index, $\lambda \geqslant 1100$ nm), the refractive index shows a low dispersion and its pressure dependence is determined mainly by that of the electronic contribution to the static dielectric constant. The obtained pressure dependence of the refractive index for long wavelengths is shown in Fig. 14. We found that the refractive index of InSe-II increases linearly under compression, being its absolute pressure derivative $\partial \ln n/\partial P = 1.8(2) \times 10^{-2}$ GPa^{-1}. This value is very close to the one observed in GaTe.

In order to understand the pressure behavior of the refractive index, we have used the Phillips-Van Vechten model.[59] In this model, the dispersion of the refractive index is given by

$$n(E) = \sqrt{1 + \frac{E_P^2}{E_O^2 - E^2}},$$

where E_P is the plasma energy of the valence electrons and E_0 is the Penn gap. From Fig. 13, we estimated both parameters: $E_P = 8.65$ eV and $E_O = 3.35$ eV. Then, since at long wavelengths the increase of the refractive index does not depend on the wavelength, we can assign the increase of the refractive index to that of $n_\infty^2 = 1 + E_P^2/E_O^2$. From this relation, and taking into account the compressibility (which enters in the pressure dependence of E_P), we can obtain the pressure dependence of the Penn gap. Unfortunately, the compressibility of the monoclinic phase of InSe is not known yet. However, it can be estimated to be between those of the γ-phase and the cubic phase of InSe. By making this assumption, we obtained that $\partial E_O/\partial P = -45$ meV/GPa. This value is at least four times smaller that the value obtained for layered phases of InSe, GaSe, and GaS in the direction perpendicular to the layers,[11] but similar to the value obtained in GaTe.[60] We think that the origin of the small pressure derivative of the Penn gap is related to the fact that, in the monoclinic structure of InSe, the In–In bonds are parallel to the layers as happens with the Ga–Ga bonds in GaTe. As we discussed above, the observed decrease in the Penn gap is a direct consequence of the pressure enhancement of the interlayer interactions.

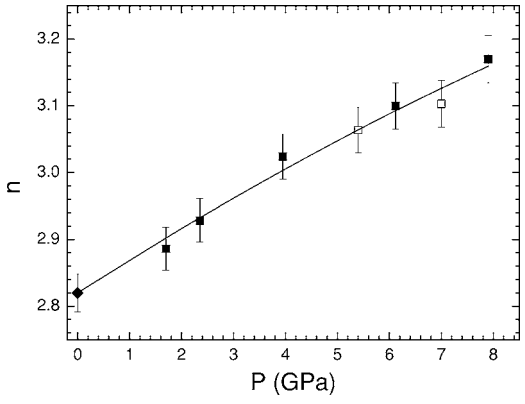

FIG. 14. Pressure dependence of the refractive index of InSe-II as obtained from the near-infrared measurements. Solid squares: Up stroke, and empty squares: Down stroke. The diamond represents a data point obtained from medium-infrared measurements.

IV. CONCLUSIONS

In the present work, we investigated the high-pressure high-temperature phase diagram of InSe; in particular, the InSe I-II phase boundary was determined up to 10 GPa. We also found evidence suggesting that InSe-II and InSe-III are metastable phases at high temperatures beyond 14 GPa, and that a new high-pressure and high-temperature phase exists above 650 K at low pressure. On top of that, by means of optical absorption measurements, we found that InSe-II is a semiconducting phase. It has an allowed direct transition with an absorption coefficient approximately ten times larger than InSe-I, which shifts to low energies upon compression. These results were analyzed on the basis of first-principles band-structure calculations which allowed us to assign the observed absorption edge to a direct transition located in the A point of the Brillouin zone. These calculations also established that InSe-II is an indirect semiconductor. However, the indirect band gap could not be obtained from our measurements due to the strong light scattering of the InSe-II samples. We also determined the refractive index of InSe-II and its pressure evolution, which has been explained trough a decrease of the Penn gap. Finally, Raman and XRD measurements were performed on InSe-II samples, and its crystalline structure was refined and its phonon modes determined.

ACKNOWLEDGMENTS

This study was supported by the MCYT of Spain under Grants No. MAT2004-05867-C03-01 and No. BFM2003-03372-C03, as well as by Generalitat de Catalunya (2005 SGR 683). One of the authors (D.E.) acknowledges financial support from the MCYT and the University of Valencia through the "Ramón y Cajal" program. Another author (G.T.) acknowledges the financial support provided through the Eu-

ropean Community's Human Potential Programme under Contract No. HPRN-CT-2002-00192, *Nanotemp*. The authors also highly appreciated the valuable comments provided by V. Muñoz on the *P-T* phase diagram of InSe. The computations described in this work were carried out using the resources of CESCA and CEPBA. The technical assistance of R. Galera and A. Mestre with the Raman and XRD measurements is also appreciated.

*Author to whom correspondence should be addressed; electronic address: daniel.errandonea@uv.es

[1] A. Segura, A. Chevy, J. P. Guesdan, and J. M. Besson, Sol. Energy Mater. **2**, 159 (1980).
[2] W. Chen, J. Burre, and D. Boucher, Laser Phys. **10**, 521 (2000).
[3] Ch. Ferrer-Roca, J. Bouvier, A. Segura, M. V. Andres, and V. Muñoz, J. Appl. Phys. **85**, 3738 (1999) and references therein.
[4] G. V. Rao, G. H. Chandra, P. S. Reddy, O. M. Hussain, K. T. R. Reddy, and S. Uthanna, J. Optoelectron. Adv. Mater. **4**, 387 (2002) and references therein.
[5] A. Koma, Thin Solid Films **216**, 72 (1992).
[6] J. F. Sanchez-Royo, A. Segura, O. Lang, E. Schaar, C. Pettenkofer, W. Jaegermann, L. Roa, and A. Chevy, J. Appl. Phys. **90**, 2818 (2001).
[7] O. Lang, R. Schlaf, Y. Tomm, C. Pettenkofer, and W. Jaegermann, J. Appl. Phys. **75**, 7805 (1994).
[8] A. Likforman, D. Carre, J. Etienne, and B. Bachet, Acta Crystallogr., Sect. B: Struct. Crystallogr. Cryst. Chem. **31**, 1252 (1975).
[9] N. Kuroda, O. Ueno, Y. Nishina, J. Phys. Soc. Jpn. **55**, 581 (1986).
[10] A. R. Goñi, A. Cantarero, U. Schwarz, K. Syassen, and A. Chevy, Phys. Rev. B **45**, 4221 (1992).
[11] D. Errandonea, A. Segura, V. Muñoz, and A. Chevy, Phys. Rev. B **60**, 15866 (1999).
[12] D. Errandonea, A. Segura, V. Muñoz, and A. Chevy, Phys. Status Solidi B **211**, 201 (1999).
[13] F. J. Manjón, D. Errandonea, A. Segura, V. Muñoz, G. Tobias, P. Ordejon, and E. Canadell, Phys. Rev. B **63**, 125330 (2001).
[14] D. Errandonea, F. J. Manjón, J. Pellicer, A. Segura, and V. Muñoz, Phys. Status Solidi B **211**, 33 (1999).
[15] G. Ferlat, H. Xu, V. Timoshevskii, and X. Blase, Phys. Rev. B **66**, 085210 (2002).
[16] K. Allahverdi, S. Babaev, S. Ellialtioglu, and A. Ismailov, Solid State Commun. **87**, 675 (1993).
[17] C. Ulrich, M. A. Mroginski, A. Goñi, A. Cantarero, U. Schwarz, V. Muñoz, and K. Syassen, Phys. Status Solidi B **198**, 121 (1996).
[18] D. Errandonea, A. Segura, J. F. Sánchez-Royo, V. Muñoz, P. Grima, A. Chevy, and C. Ulrich, Phys. Rev. B **55**, 16217 (1997).
[19] D. Errandonea, J. F. Sánchez-Royo, A. Segura, A. Chevy, and L. Roa, High Press. Res. **16**, 13 (1998).
[20] J. F. Sánchez Royo, D. Errandonea, A. Segura, A. Chevy, and L. Roa, J. Appl. Phys. **83**, 4750 (1998).
[21] D. Errandonea, A. Segura, J. F. Sánchez Royo, V. Muñoz, C. Ulrich, P. Grima, and A. Chevy, Phys. Status Solidi B **198**, 129 (1996).
[22] D. Errandonea, A. Segura, F. J. Manjón, and A. Chevy, Semicond. Sci. Technol. **18**, 241 (2003).
[23] D. Errandonea, A. Segura, F. J. Manjón, A. Chevy, E. Machado, G. Tobias, P. Ordejon, and E. Canadell, Phys. Rev. B **71**, 125206 (2005).
[24] U. Schwarz, A. R. Goñi, K. Syassen, A. Cantarero, and A. Chevy, High Press. Res. **8**, 396 (1991).
[25] F. J. Manjon, D. Errandonea, A. Segura, J. C. Chervin, and V. Muñoz, High Press. Res. **22**, 261 (2002).
[26] H. Iwasaki, Y. Watanabe, N. Kuroda, and Y. Nishina, Physica B & C **105B**, 314 (1981).
[27] G. C. Vezzoli, Mater. Res. Bull. **6**, 1201 (1971).
[28] G. Ferlat, D. Martinez-Garcia, A. San-Miguel, A. Aouizerat, and V. Muñoz, High Press. Res. **24**, 111 (2004).
[29] N. Kuroda, Y. Nishina, H. Iwasaki, and Y. Watanabe, Solid State Commun. **38**, 139 (1981).
[30] A. Chevy, J. Cryst. Growth **67**, 119 (1984).
[31] H. K. Mao, J. Xu, and P. Bell, J. Geophys. Res. **91**, 4673 (1986).
[32] F. Datchi, R. Le Toulec, and P. Loubeyre, J. Appl. Phys. **81**, 3333 (1997).
[33] D. Errandonea, B. Schwager, R. Ditz, C. Gessmann, R. Boehler, and M. Ross, Phys. Rev. B **63**, 132104 (2001).
[34] A. K. Bandyopadhya, S. Chatterjee, E. S. R. Gopal, and S. V. Subramanyam, Rev. Sci. Instrum. **32**, 1232 (1981).
[35] M. Nishikawa and S. Akimoto, High Temp. - High Press. **3**, 161 (1971).
[36] F. P. Bundy, J. Appl. Phys. **32**, 483 (1961).
[37] J. L. van der Pauw, Philips Res. Rep. **13**, 1 (1958).
[38] P. Hohenberg and W. Kohn, Phys. Rev. **136**, 864 (1964); W. Kohn and L. J. Sham, *ibid.* **140**, 1133 (1965).
[39] J. M. Soler, E. Artacho, J. D. Gale, A. García, J. Junquera, P. Ordejón, and D. Sánchez-Portal, J. Phys.: Condens. Matter **14**, 2745 (2002).
[40] J. P. Perdew and A. Zunger, Phys. Rev. B **23**, 5048 (1981).
[41] N. Troullier and J. L. Martins, Phys. Rev. B **43**, 1993 (1991).
[42] L. Kleinman and D. M. Bylander, Phys. Rev. Lett. **48**, 1425 (1982).
[43] S. G. Louie, S. Froyen, and M. L. Cohen, Phys. Rev. B **26**, 1738 (1982).
[44] E. Artacho, D. Sánchez-Portal, P. Ordejón, A. García, and J. M. Soler, Phys. Status Solidi B **215**, 809 (1999).
[45] H. J. Monkhorst and J. D. Pack, Phys. Rev. B **13**, 5188 (1976).
[46] D. Hull and D. J. Bacon, *Introduction to Dislocations, International Series of Materials Science and Technology*, Vol. 37 (Pergamon Press, Oxford, 1984).
[47] D. Errandonea, B. Schwager, R. Boehler, and M. Ross, Phys. Rev. B **65**, 214110 (2002).
[48] D. Errandonea, R. Boehler, S. Japel, M. Mezouar, and L. R. Benedetti, Phys. Rev. B **73**, 092106 (2006).
[49] D. V. Schroeder, *An Introduction to Thermal Physics* (Addison–Wesley, Reading, MA, 1999).
[50] L. D. Landau and E. M. Lifshitz, *Statistical Physics* (Pergamon, London, 1958).
[51] S. Inoue, T. Yoshida, and T. Morita, Jpn. J. Appl. Phys., Part 1 **21**, 242 (1982).

[52] C. De Blasi, D. Manno, and A. Rizzo, J. Cryst. Growth **100**, 347 (1990).
[53] M. Julien-Pouzol, S. Jaulmes, M. Guittard, and F. Alapini, Acta Crystallogr. **35**, 2848 (1979).
[54] W. Kraus and G. Nolze, J. Appl. Crystallogr. **29**, 301 (1996).
[55] N. M. Gasanly, B. M. Yavadov, V. I. Tagirov, and E. A. Vonogradov, Phys. Status Solidi B **89**, K43 (1978).
[56] N. Kuroda and Y. Nishina, Solid State Commun. **28**, 439 (1978); **30**, 95 (1979); **34**, 481 (1980).
[57] L. N. Alieva, G. L. Belenkii, I. I. Reshina, E. Yu Salaev, and V. Ya Shteinshraiber, Speech Technol. **21**, 90 (1979).
[58] F. E. Faradev, N. M. Gasanly, B. N. Mavrin, and N. N. Melnik, Phys. Status Solidi B **85**, 381 (1978).
[59] G. Martinez, in *Handbook of Semiconductors*, edited by J. S. Moss and M. Balkanski (North–Holland, Amsterdam, 1980), Vol. 2, p. 181.
[60] J. Pellicer-Porres, A. Segura, V. Muñoz, and J. C. Chervin, Semicond. Sci. Technol. **15**, 902 (2000).